

Investigation of signal-to-noise ratio in frequency-domain multiphoton fluorescence lifetime imaging microscopy

YIDE ZHANG, AAMIR A. KHAN, GENEVIEVE D. VIGIL, AND SCOTT S. HOWARD*

Department of Electrical Engineering, University of Notre Dame, Notre Dame, Indiana 46556, USA

*Corresponding author: showard@nd.edu

Received 22 December 2015; revised 5 April 2016; accepted 6 April 2016; posted 7 April 2016 (Doc. ID 256231); published 2 May 2016

Multiphoton microscopy (MPM) combined with fluorescence lifetime imaging microscopy (FLIM) has enabled three-dimensional quantitative molecular microscopy *in vivo*. The signal-to-noise ratio (SNR), and thus the imaging rate of MPM-FLIM, which is fundamentally limited by the shot noise and fluorescence saturation, has not been quantitatively studied yet. In this paper, we investigate the SNR performance of the frequency-domain (FD) MPM-FLIM with two figures of merit: the photon economy in the limit of shot noise, and the normalized SNR in the limit of saturation. The theoretical results and Monte Carlo simulations find that two-photon FD-FLIM requires 50% fewer photons to achieve the same SNR as conventional one-photon FLIM. We also analytically show that the MPM-FD-FLIM can exploit the DC and higher harmonic components generated by nonlinear optical mixing of the excitation light to improve SNR, reducing the required number of photons by an additional 50%. Finally, the effect of fluorophore saturation on the experimental SNR performance is discussed. © 2016 Optical Society of America

OCIS codes: (180.4315) Nonlinear microscopy; (190.4180) Multiphoton processes; (170.2520) Fluorescence microscopy; (170.3650) Lifetime-based sensing.

<http://dx.doi.org/10.1364/JOSAA.33.0000B1>

1. INTRODUCTION

Multiphoton microscopy (MPM) is a widely used *in vivo* imaging technique in biological and medical applications [1–7]. In the case of two-photon excitation (2PE) fluorescence microscopy, two excitation photons excite a fluorophore, which in turn emits a single higher-energy photon [1]. The rate of 2PE depends quadratically on the excitation intensity, thus enabling the axial localization of excitation in the vicinity of the focal plane [8]. The 2PE generally uses near-infrared excitation, which experiences less scattering in tissue than shorter-wavelength light and does not cause background autofluorescence. Therefore, out-of-focus fluorescence is avoided, and the overall photobleaching and phototoxicity in thick samples are reduced [9–14].

Fluorescence lifetime imaging microscopy (FLIM) is also a powerful tool in biological, chemical, and medical studies: it provides an additional contrast in optical microscopy by measuring the fluorescence decay lifetime of excited fluorophores [15–20]. For example, FLIM can be employed to image local Ca^{2+} or K^+ ion concentrations, dissolved oxygen concentrations, pH, refractive index, or the occurrence of fluorescence resonance energy transfer [19,21,22]. Compared with fluorescence emission intensity microscopy, FLIM has the advantage

of significantly reduced sensitivity to errors caused by non-uniform optical absorption, scattering, photobleaching, fluctuations in fluorophore concentration, and drift in detector sensitivity and excitation power [23–25]. The variety of imaging methods developed to extract fluorophore lifetime from a sample can be divided into two categories: time-domain (TD) and frequency-domain (FD) techniques. TD methods, such as time-correlated single photon counting, time-gating, and analog mean delay, obtain the lifetime information by exciting the sample with short optical pulses and measuring the temporal distribution of emission fluorescence [17,21,26,27]. FD methods, on the other hand, rely on the relative delay of periodic intensity-modulated excitation light to obtain lifetime images. FD methods are often preferred because of their relatively rapid acquisition speed and simpler electronics, while eliminating the requirement for the short pulses needed in TD methods [23,28].

The MPM and FLIM techniques can be combined into an integrated imaging system that possesses not only the advantages of MPM, such as high signal-to-noise ratio (SNR) and large imaging depth, but also the strengths of FLIM, including error tolerance and the ability to discriminate different fluorophores with similar emission spectra. FLIM and MPM have

been employed to produce *in vivo* lifetime images with high spatial and temporal resolutions [29,30], high pixel rates [31], and large depth penetration [32].

The SNRs of MPM and FLIM are each fundamentally limited by photon quantum noise or shot noise [16,33]. This noise comes from the intrinsic nature of the photon emission and cannot be eliminated from the measurement system [24]. Other noise sources, such as electronic noise and multiplicative noise in photomultipliers, will influence the imaging results as well, but their influences are negligible compared to shot noise or can be eliminated with digital acquisition [34,35]. While the SNR can be improved by increasing the number of detected photons [27], technical limitations arise due to the excessive acquisition time, increased photobleaching, and blurred images due to sample movement [23,36].

When comparing FLIM techniques, the photon economy, or the F -value, is a widely used figure of merit to compare SNRs [18]. It is described as the normalized RMS noise in lifetime acquisition where the normalization is based on an ideal photon quantum noise-limited intensity measurement [23,33]. Higher F -values indicate noisier lifetime acquisitions and hence poorer SNR performances. The best theoretically achievable F -value is 1, where the lifetime measurement itself is limited by the photon quantum noise. FLIM techniques with a poor photon economy require a higher (F^2 -fold) number of photons than an ideal efficient system ($F = 1$) to achieve the same uncertainty level in lifetime imaging, which means that longer acquisition times are needed for these techniques [37]. Though many research efforts have been conducted to investigate the F -value for the conventional single photon FLIM [23,24,33,37], the SNR performance of MPM-FLIM has not been quantitatively studied yet. In this paper, we discuss the SNR figures of merit of MPM-FD-FLIM for various excitation techniques with analytical derivations and Monte Carlo simulations. In Section 4, we find that MPM-FLIM requires 50% fewer photons to achieve the same efficiency as conventional one-photon microscopy.

FLIM SNR is a function of both excitation waveform as well as lock-in detection techniques [36]. The imaging systems discussed in this paper only use lock-in detection, which generally shows better photon economy over other FD-FLIM detection techniques such as image intensifiers [23,35]. Generally, the lock-in amplifier is tuned solely to the fundamental excitation modulation. In this paper, we show that the DC or higher harmonics of the fluorescent light can also be used for lifetime imaging. Although it has been previously shown that exploiting higher harmonics to measure lifetime results in extremely high F -values, and thus a very poor SNR performance [33,37], we show in Section 5 that exploiting the DC signal with lock-in detection of FD-FLIM can further reduce the number of photons needed in FLIM by an additional 50%.

Finally, in Section 6, we investigate SNR under a practical situation where 2PE microscopes operate at as high of an excitation rate as possible to achieve maximum SNR while avoiding saturation, for saturation could complicate the excited-state dynamics and alter the measured lifetime. We conclude this paper with a guideline for experimentalists using MPM-FD-FLIM.

2. SYSTEM MODELING

The MPM-FD-FLIM system will be modeled similar to the method described in Ref. [23], where time variables are scaled to be dimensionless to simplify the analysis. Unscaled time variables are presented with an asterisk *, including the time t^* , average fluorescence lifetime τ^* , and modulation period $T^* = 2\pi/\omega$. After scaling, these time variables become t , τ , and T , respectively. The scaling relations are $t = \omega t^*$, $\tau = \omega \tau^*$, and $T = 2\pi$.

The setup of this imaging system can be modeled as follows. A mode-locked laser is used as the excitation source. An electro-optical modulator (EOM) is used to intensity modulate the light, generating the modulated exciting light $e(t)$. The modulation waveforms for the EOM are controlled by an arbitrary function generator. The sample is then excited by $e(t)$ and generates 2PE fluorescence $p(t)$. With the strict quadratic dependence on excitation light [8,13,25], the two-photon fluorescence $p(t)$ is the convolution of $e^2(t)$ and $f(t)$, where

$$f(t) = \frac{1}{\tau} \exp\left(-\frac{t}{\tau}\right), \quad t \geq 0, \quad (1)$$

is the impulse response of the unsaturated fluorophore, which is normalized such that its integral on the time domain $t \geq 0$ is unity. We define the effective excitation light as $\varepsilon(t) = e^2(t)$, which will be used in the following analysis.

The effective excitation light is periodic; therefore, it can be expanded into a Fourier series as follows:

$$\begin{aligned} \varepsilon(t) = e^2(t) &= \sum_{k=-\infty}^{+\infty} a_k \exp(ikt) \\ a_k &= \frac{1}{2\pi} \int_0^{2\pi} \varepsilon(t) \exp(-ikt) dt, \quad k = 0, \pm 1, \pm 2, \dots, \end{aligned} \quad (2)$$

where a_k are the corresponding Fourier coefficients. Being periodic as well, the fluorescence light and its Fourier coefficients are given by

$$\begin{aligned} p(t) = \varepsilon(t) * f(t) &= \sum_{k=-\infty}^{+\infty} d_k \exp(ikt) \\ d_k &= a_k \frac{1}{1 + ik\tau}, \quad k = 0, \pm 1, \pm 2, \dots, \end{aligned} \quad (3)$$

where the Convolution Theorem is used to find d_k .

The frequency components of the detected signal $p(t)$ are extracted by lock-in detection or Fourier analysis. These components contain the information about τ . Since the collected signal is real, the analysis is simplified by limiting the frequency domain to non-negative frequencies. For the n th harmonic component, i.e., lock-in frequency $n\omega$, the corresponding complex Fourier coefficient is

$$d_n = \frac{1}{2\pi} \int_0^{2\pi} p(t) \exp(-int) dt, \quad n = 0, 1, 2, \dots \quad (4)$$

Its real and imaginary parts, corresponding to the Fourier cosine transform (G) and Fourier sine transform (S), respectively, are

$$\begin{cases} G_n = \text{Re}\{d_n\} = \frac{1}{2\pi} \int_0^{2\pi} p(t) \cos(nt) dt, \\ S_n = \text{Im}\{d_n\} = -\frac{1}{2\pi} \int_0^{2\pi} p(t) \sin(nt) dt, \end{cases} \quad n = 0, 1, 2, \dots \quad (5)$$

With Eq. (3), G_n and S_n can be related to a_n by

$$\begin{cases} G_n = \text{Re}\{a_n\} \frac{1}{1+n^2\tau^2} + \text{Im}\{a_n\} \frac{-n\tau}{1+n^2\tau^2}, \\ S_n = \text{Re}\{a_n\} \frac{-n\tau}{1+n^2\tau^2} + \text{Im}\{a_n\} \frac{1}{1+n^2\tau^2}, \end{cases} \quad n = 0, 1, 2, \dots \quad (6)$$

By solving Eq. (6), one can obtain τ . However, solving Eq. (6) would be a laborious task if both $\text{Re}\{a_n\}$ and $\text{Im}\{a_n\}$ are non-zero. So in order to calculate τ efficiently, a_n should be either purely real or purely imaginary. When a_n is real, $\tau = -(1/n)(S_n/G_n)$, and when a_n is imaginary, $\tau = (1/n)(G_n/S_n)$. Therefore, lifetime τ can be obtained not only from the fundamental component (lock-in frequency ω), but also from the combination of the other n th-order harmonics generated by non-linear mixing, since all of them, except the DC, contain the information about τ .

3. FIGURES OF MERIT

The photon economy (F -value) is a widely used figure of merit for comparing the SNR of FLIM systems. In this paper, we will describe systems in terms of the photon economy as well as present a new figure of merit based on the saturation-normalized SNR to compare the FLIM performance when it is limited by fluorescence saturation, as is common in long-lifetime (phosphorescent) systems.

A. Photon Economy

The photon economy (F -value) is defined as the ratio of the uncertainty in lifetime (τ) acquisition to the one in intensity (I) measurement, with the same amount of detected photons [18]. $F = (\sigma_\tau/\tau)/(\sigma_I/I)$, where σ_τ and σ_I are the standard deviations of the experimentally measured lifetime and intensity, respectively. If we denote the intensity I as N_{det} , the number of photons detected in a measurement, which is Poisson distributed [23], then the standard deviation σ_I is $\sqrt{N_{\text{det}}}$. Therefore, the F -value is

$$F = \sqrt{N_{\text{det}}} \frac{\sigma_\tau}{\tau}. \quad (7)$$

F now quantifies the sensitivity of the lifetime acquisition approach. F is limited to $F > 1$ due to shot noise; $F = 1$ in an ideal shot-noise-limited FLIM system. The F -value can also be considered as the ratio between the ideal photon quantum noise-limited SNR ($\sqrt{N_{\text{det}}}$) and the measurement SNR (τ/σ_τ) [24]. F^2 represents the relative number of photons required (e.g., the decrease in the measurement rate) compared to an ideal photon quantum noise-limited case [33] for a desired SNR.

B. Saturation Normalized Signal-to-Noise Ratio

The fluorescent lifetime SNR is expressed as

$$\frac{\tau}{\sigma_\tau} = \frac{\sqrt{N_{\text{det}}}}{F} = \frac{\sqrt{T_m R}}{F}, \quad (8)$$

where R is the photon generation rate and T_m is the total measurement time. However, R is fundamentally limited

by the fluorescence saturation, which in turn is limited by the fluorescence lifetime. Since R and F are the fundamental limits and properties of a lifetime measurement system while T_m is arbitrary, a straightforward figure of merit for comparing a saturation-limited FLIM system can be given by:

$$\overline{\text{SNR}} = \frac{\sqrt{R}}{F} = \frac{\sqrt{N_{\text{det}}}}{F\sqrt{T_m}}. \quad (9)$$

This is similar to the approach of another figure of merit, relative throughput, as introduced in Ref. [37] to account for not only the efficiency, but also the acquisition speed of a microscope.

4. EXCITATION SIGNAL-TO-NOISE RATIO ANALYSIS

In this section, FLIM figures of merit are calculated for various excitation waveforms via analytical calculation and numerical Monte Carlo simulations. In this first analysis of excitation waveforms, we limit the analysis to the fundamental harmonic component, i.e., 1ω .

Theoretically, we use an error-propagation method introduced in Ref. [23], which applies if the lifetime τ can be written in the following form:

$$\tau = \frac{U}{V} = \frac{\mu_1 + \sigma_1 Y_1}{\mu_2 + \sigma_2 Y_2}, \quad (10)$$

where U and V are random variables, Y_1 and Y_2 are auxiliary random variables with zero mean and unity variance, μ_1 and μ_2 are the means; and σ_1 and σ_2 are the standard deviations of U and V , respectively. In practice, $\sigma_1^2 \approx E[U^2]$ and $\sigma_2^2 \approx E[V^2]$. Now denote the coefficients of variation as $\delta_1 = \sigma_1/\mu_1$ and $\delta_2 = \sigma_2/\mu_2$, and assume that the absolute value of δ_2 is smaller than one. Equation (10) is expanded as

$$\tau = \frac{\mu_1}{\mu_2} (1 + \delta_1 Y_1 - \delta_2 Y_2 - \delta_1 \delta_2 Y_1 Y_2 + \delta_2^2 Y_2^2 + \dots). \quad (11)$$

Unless otherwise specified, we omit the moments of order larger than 2 in the following analysis, for their contribution to the final results is small [36]. Therefore, we get the expected value of τ as

$$E[\tau] = \frac{\mu_1}{\mu_2} (1 - \rho \delta_1 \delta_2 + \delta_2^2), \quad (12)$$

where $\rho = E[Y_1 Y_2]$ is the correlation coefficient of U and V . From Eq. (11), we also have

$$E[\tau^2] = \left(\frac{\mu_1}{\mu_2}\right)^2 (1 + \delta_1^2 + 3\delta_2^2 - 4\rho\delta_1\delta_2). \quad (13)$$

Consequently, the variance of τ is

$$\sigma_\tau^2 = E[\tau^2] - E[\tau]^2 = \left(\frac{\mu_1}{\mu_2}\right)^2 (\delta_1^2 + \delta_2^2 - 2\rho\delta_1\delta_2). \quad (14)$$

The theoretical figures of merit can then be calculated using Eqs. (7) and (9).

Additionally, we use Monte Carlo simulations to verify the analytical results. The Monte Carlo simulations are done by dividing each modulation period ($T = 2\pi$) into M time units $\Delta t = 2\pi/M$ [23,33,35]. The number M is sufficiently large (here, $M = 30000$) to keep the probability of several photons

emitting in a time unit small, thus ignoring the piling-up effect [38]. In each unit, a uniformly distributed random number between 0 and 1 is generated and compared with the probability density described by the product of the fluorescent light intensity $p(t)$ in Eq. (3) and the time unit Δt . If the generated random number is smaller than $p(t)\Delta t$, it will be regarded as a fluorescent photon having been emitted. Then, the detector will cumulatively record the detected photons and extract the lifetime information in each measurement (i.e., N_{mod} periods, here, $N_{\text{mod}} = 2400$) based on the lock-in technique in use. The measurement process is repeated 1000 times to generate a set of output values, including the acquired lifetime τ and the total number of detected photons N_{det} . Following this, a statistical analysis is performed to find the means and variances of these outputs, and the figures of merit are obtained accordingly.

A. Square Root of Sinusoid

First, we observe the performance of a modulation waveform of the square root of a sinusoidal function. After the 2PE fluorescence process, the effective excitation light has a waveform of a sinusoidal function. In this way, the two-photon fluorescent emission that the fluorophore in the sample experiences is equivalent to a one-photon process with a sinusoidally modulated excitation light, which has been studied in Ref. [23]. The resulting performances of these two processes are expected to be the same and thus can be used to compare to linear excitation. The illumination light is

$$e(t) = \frac{1}{\sqrt{2\pi}} [1 + m \sin(t)]^{\frac{1}{2}}, \quad (15)$$

where m is the degree of modulation, $0 < m \leq 1$. With the 2PE process, the effective exciting light is

$$\varepsilon(t) = \frac{1}{2\pi} [1 + m \sin(t)], \quad (16)$$

which has the first harmonic Fourier coefficient

$$a_1 = -\frac{m}{4\pi} i. \quad (17)$$

Correspondingly, the fluorescence $p(t)$ has the first harmonics

$$G_1 = -\frac{m}{4\pi} \frac{\tau}{1 + \tau^2}, \quad S_1 = -\frac{m}{4\pi} \frac{1}{1 + \tau^2}. \quad (18)$$

Therefore, the lifetime can be acquired from $\tau = G_1/S_1$. Equations (15) and (16) have been normalized to guarantee that the integral of the fluorescence in a modulation period is unified,

$$\int_0^{2\pi} p(t) dt = 1. \quad (19)$$

Thus, on average, only one photon is emitted in every period; i.e., the 2PE emission rate is assumed to be constant. This assumption is feasible because the problem under investigation is a scaled one; it can be recovered to realistic situations once the modulation frequency ω is included.

$p(t)$ can be regarded as the probability density function of detecting a photon. For a random variable X in the detector, if its realization is based on detecting a photon, then its expected value in a modulation period, or for each emitting photon, is

$$E[X] = \int_0^{2\pi} X p(t) dt. \quad (20)$$

In each measurement, N_{det} photons are detected. Therefore, the expected value for X in one measurement is $N_{\text{det}}E[X]$. Denote the random processes corresponding to G_1 and S_1 in the lock-in detector as X_{G_1} and X_{S_1} , respectively. Then, for the square root of sinusoidal modulation, the expected value of the acquired lifetime τ is

$$\bar{\tau} = \frac{N_{\text{det}}E[X_{G_1}]}{N_{\text{det}}E[X_{S_1}]} \quad (21)$$

With the definition of Fourier transforms and from Eq. (5), we know that

$$X_{G_1} = \cos(t), \quad X_{S_1} = -\sin(t). \quad (22)$$

So, the expected values for them are

$$E[X_{G_1}] = \int_0^{2\pi} p(t) \cos(t) dt = 2\pi G_1, \quad (23)$$

$$E[X_{S_1}] = -\int_0^{2\pi} p(t) \sin(t) dt = 2\pi S_1. \quad (24)$$

Based on Eqs. (10)–(14), in this case, we have $U = G_1$, $V = S_1$, and

$$\begin{aligned} \mu_1 &= E[U] = N_{\text{det}}E[X_{G_1}] = -N_{\text{det}} \frac{m}{2} \frac{\tau}{1 + \tau^2}, \\ \mu_2 &= E[V] = N_{\text{det}}E[X_{S_1}] = -N_{\text{det}} \frac{m}{2} \frac{1}{1 + \tau^2}. \end{aligned} \quad (25)$$

The variances and the correlation coefficient are

$$\begin{aligned} \sigma_1^2 &= E[U^2] = N_{\text{det}}E[X_{G_1}^2], \\ \sigma_2^2 &= E[V^2] = N_{\text{det}}E[X_{S_1}^2], \\ \rho\sigma_1\sigma_2 &= E[UV] = N_{\text{det}}E[X_{G_1}X_{S_1}], \end{aligned} \quad (26)$$

where, from Eq. (5),

$$E[X_{G_1}^2] = E[\cos^2(t)] = \frac{1}{2} (1 + 2\pi G_2), \quad (27)$$

$$E[X_{S_1}^2] = E[\sin^2(t)] = \frac{1}{2} (1 - 2\pi G_2), \quad (28)$$

$$E[X_{G_1}X_{S_1}] = E[-\cos(t)\sin(t)] = \frac{1}{2} 2\pi S_2. \quad (29)$$

Since a_2 of the effective exciting light [Eq. (16)] is 0, $G_2 = 0$, $S_2 = 0$ from Eq. (6). Therefore,

$$\sigma_1^2 = \frac{1}{2} N_{\text{det}}, \quad \sigma_2^2 = \frac{1}{2} N_{\text{det}}, \quad \rho\sigma_1\sigma_2 = 0. \quad (30)$$

From Eq. (14), we obtain the standard deviation of the lifetime,

$$\sigma_\tau = \sqrt{\frac{2}{N_{\text{det}}} \frac{(1 + \tau^2)^{\frac{3}{2}}}{m}}. \quad (31)$$

Consequently, the F -value is

$$F = \sqrt{N_{\text{det}}} \frac{\sigma_\tau}{\tau} = \sqrt{2} \frac{(1 + \tau^2)^{\frac{3}{2}}}{m\tau}. \quad (32)$$

The normalized SNR, from Eq. (9), is

$$\overline{\text{SNR}} = \frac{\sqrt{N_{\text{det}}}}{F} \frac{1}{\sqrt{2\pi N_{\text{mod}}}} = \sqrt{\frac{N_{\text{det}}}{N_{\text{mod}} F^2 2\pi}}, \quad (33)$$

where N_{mod} is the number of modulation periods in a measurement. Since in this analysis, each period, on average, emits one photon, $N_{\text{det}} = N_{\text{mod}}$, then

$$\overline{\text{SNR}} = \frac{1}{F\sqrt{2\pi}}. \quad (34)$$

The theoretical results in Eq. (32) are plotted as curves, with the variance of the degree of modulation m , in Fig. 1, where the corresponding Monte Carlo simulation results are also plotted as dots. Figure 1 shows the agreement between the theoretical derivations and Monte Carlo simulations. All these F -values are plotted as a function of the modulation frequency, which has a unit of $1/\tau^*$, essentially, Hz. As can be read from the figure, the best F -value is $F = 3.67$, corresponding to $\overline{\text{SNR}} = 0.11$ for $m = 1$ at the frequency of $0.11/\tau^*$. This result is in accordance with expectation, as it is the same with the F -value reported in Ref. [23] for the sinusoidally modulated one-photon process. Also, as the degree of modulation m goes down, the figures of merit get worse. This calls for a high degree of modulation for the exciting light in real experiments.

B. Sinusoid

A sinusoidally modulated exciting light is common in use and easy to produce. With the same normalization criterion for $p(t)$ in Eq. (19), the illumination and the corresponding effective excitation light signals are

$$e(t) = \frac{1}{\sqrt{\pi(m^2 + 2)}} [1 + m \sin(t)], \quad (35)$$

$$\varepsilon(t) = \frac{1}{2\pi(m^2 + 2)} [m^2 + 2 + 4m \sin(t) - m^2 \cos(2t)], \quad (36)$$

where m is the degree of modulation $0 < m \leq 1$. The first harmonic Fourier coefficient of $\varepsilon(t)$ is

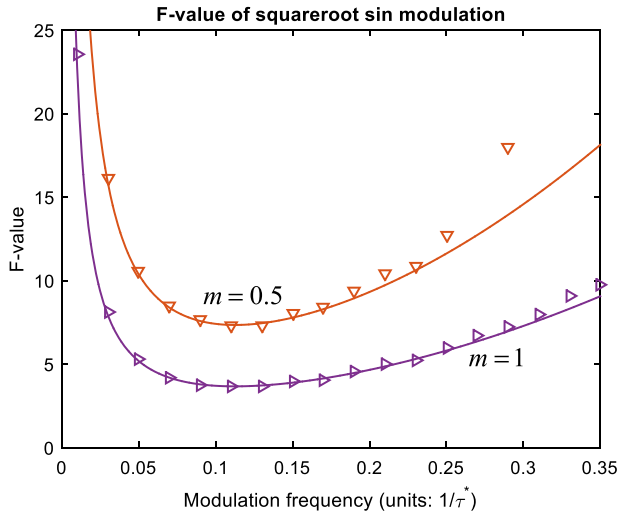


Fig. 1. F -value as a function of the modulation frequency with the first harmonic frequency (1ω) lock-in detection for square-root sinusoidally modulated excitation light.

$$a_1 = -\frac{m}{\pi(m^2 + 2)} i. \quad (37)$$

Then, from Eq. (6), we have

$$G_1 = -\frac{m}{\pi(m^2 + 2)} \frac{\tau}{1 + \tau^2}, \quad S_1 = -\frac{m}{\pi(m^2 + 2)} \frac{1}{1 + \tau^2}. \quad (38)$$

Consequently, the lifetime is also obtained by $\tau = G_1/S_1$, which shares the same form with Eq. (10). The derivation is the same with Eqs. (10)–(14), where we have $U = G_1$, $V = S_1$, and with Eqs. (22)–(24),

$$\begin{aligned} \mu_1 &= E[U] = N_{\text{det}} E[X_{G_1}] = -N_{\text{det}} \frac{2m}{m^2 + 2} \frac{\tau}{1 + \tau^2}, \\ \mu_2 &= E[V] = N_{\text{det}} E[X_{S_1}] = -N_{\text{det}} \frac{2m}{m^2 + 2} \frac{1}{1 + \tau^2}. \end{aligned} \quad (39)$$

Equations (27)–(29) require the knowledge of the second harmonic Fourier coefficients, which are

$$\begin{aligned} a_2 &= -\frac{m^2}{4\pi(m^2 + 2)}, \\ G_2 &= -\frac{m^2}{4\pi(m^2 + 2)} \frac{1}{1 + 4\tau^2}, \quad S_2 = \frac{m^2}{4\pi(m^2 + 2)} \frac{2\tau}{1 + 4\tau^2}. \end{aligned} \quad (40)$$

Therefore, the second moments are

$$\begin{aligned} \sigma_1^2 &= E[U^2] = N_{\text{det}} E[X_{G_1}^2] = N_{\text{det}} \left[\frac{1}{2} - \frac{m^2}{4(m^2 + 2)} \frac{1}{1 + 4\tau^2} \right], \\ \sigma_2^2 &= E[V^2] = N_{\text{det}} E[X_{S_1}^2] = N_{\text{det}} \left[\frac{1}{2} + \frac{m^2}{4(m^2 + 2)} \frac{1}{1 + 4\tau^2} \right], \\ \rho\sigma_1\sigma_2 &= E[UV] = N_{\text{det}} E[X_{G_1}X_{S_1}] = N_{\text{det}} \frac{m^2}{4(m^2 + 2)} \frac{2\tau}{1 + 4\tau^2}. \end{aligned} \quad (41)$$

Then, from Eq. (14), the standard deviation of τ is obtained,

$$\begin{aligned} \sigma_\tau &= \frac{1 + \tau^2}{4m} \left(\frac{1}{N_{\text{det}}} \frac{m^2 + 2}{1 + 4\tau^2} \right)^{\frac{1}{2}} \\ &\quad \times (4 + m^2 + 7m^2\tau^2 + 20\tau^2 + 8m^2\tau^4 + 16\tau^4)^{\frac{1}{2}}. \end{aligned} \quad (42)$$

So the F -value is

$$\begin{aligned} F &= \frac{1 + \tau^2}{4m\tau} \left(\frac{m^2 + 2}{1 + 4\tau^2} \right)^{\frac{1}{2}} \\ &\quad \times (4 + m^2 + 7m^2\tau^2 + 20\tau^2 + 8m^2\tau^4 + 16\tau^4)^{\frac{1}{2}}, \end{aligned} \quad (43)$$

and the normalized SNR has the same form as Eq. (34). The derived and Monte Carlo simulated F -values are plotted in Fig. 2. The best figures of merit are $F = 2.62$, $\overline{\text{SNR}} = 0.15$ for $m = 1$ at the frequency of $0.11/\tau^*$. And the figures of merit are getting worse as the degree of modulation goes down. Therefore, a high degree of modulation is also required in this case.

C. Periodic Square Wave and Dirac Comb

Excitation by a periodic square wave, or ideally a Dirac comb when the duty cycle is zero, though it requires a large system bandwidth, is preferable in FLIM. The same normalization for

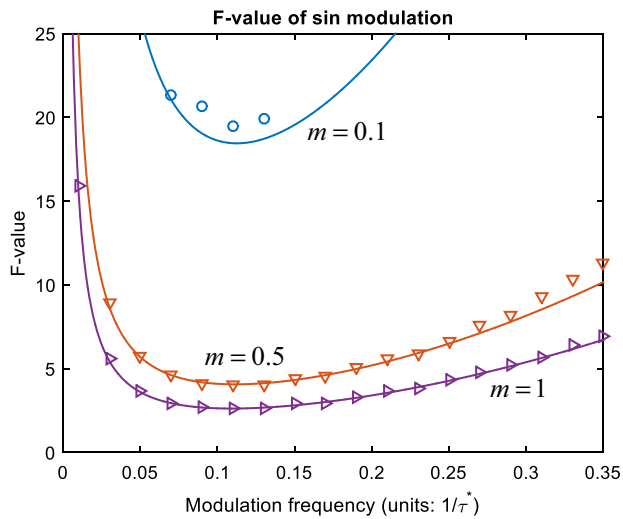


Fig. 2. F -value as a function of the modulation frequency with the first harmonic frequency (ω) lock-in detection for sinusoidally modulated excitation light.

$p(t)$ in Eq. (19) results in the excitation and the effective excitation light signals as

$$e(t) = \sum_{k=-\infty}^{\infty} \frac{1}{\sqrt{2\pi a}} [\theta(t - 2\pi k + \pi a) - \theta(t - 2\pi k - \pi a)], \quad (44)$$

$$\varepsilon(t) = \sum_{k=-\infty}^{\infty} \frac{1}{2\pi a} [\theta(t - 2\pi k + \pi a) - \theta(t - 2\pi k - \pi a)], \quad (45)$$

where a is the duty cycle $0 \leq a \leq 1$, and $\theta(\cdot)$ is the unit step function. The first harmonic Fourier coefficient of $\varepsilon(t)$ is

$$a_1 = \frac{1}{2\pi} \frac{\sin(\pi a)}{\pi a}, \quad (46)$$

and with Eq. (6),

$$G_1 = \frac{1}{2\pi} \frac{\sin(\pi a)}{\pi a} \frac{1}{1 + \tau^2}, \quad S_1 = -\frac{1}{2\pi} \frac{\sin(\pi a)}{\pi a} \frac{\tau}{1 + \tau^2}. \quad (47)$$

So the lifetime can be extracted by $\tau = -S_1/G_1$. With the same derivations as Eqs. (10)–(14), we have $U = -S_1$, $V = G_1$. Equations (22)–(24) still hold, but since U and V have changed, we get

$$\begin{aligned} \mu_1 &= E[U] = -N_{\text{det}} E[X_{S1}] = N_{\text{det}} \frac{\sin(\pi a)}{\pi a} \frac{\tau}{1 + \tau^2}, \\ \mu_2 &= E[V] = N_{\text{det}} E[X_{G1}] = N_{\text{det}} \frac{\sin(\pi a)}{\pi a} \frac{1}{1 + \tau^2}. \end{aligned} \quad (48)$$

The second harmonic Fourier coefficients are

$$\begin{aligned} a_2 &= \frac{1}{2\pi} \frac{\sin(2\pi a)}{2\pi a}, \quad G_2 = \frac{1}{2\pi} \frac{\sin(2\pi a)}{2\pi a} \frac{1}{1 + 4\tau^2}, \\ S_2 &= -\frac{1}{2\pi} \frac{\sin(2\pi a)}{2\pi a} \frac{2\tau}{1 + 4\tau^2}, \end{aligned} \quad (49)$$

giving the second moments, according to Eqs. (27)–(29), as

$$\begin{aligned} \sigma_1^2 &= E[U^2] = N_{\text{det}} E[X_{S1}^2] = N_{\text{det}} \left[\frac{1}{2} - \frac{\sin(2\pi a)}{4\pi a} \frac{1}{1 + 4\tau^2} \right], \\ \sigma_2^2 &= E[V^2] = N_{\text{det}} E[X_{G1}^2] = N_{\text{det}} \left[\frac{1}{2} + \frac{\sin(2\pi a)}{4\pi a} \frac{1}{1 + 4\tau^2} \right], \\ \rho\sigma_1\sigma_2 &= E[UV] = N_{\text{det}} \{-E[X_{G1}X_{S1}]\} = N_{\text{det}} \frac{\sin(2\pi a)}{4\pi a} \frac{2\tau}{1 + 4\tau^2}. \end{aligned} \quad (50)$$

Then, from Eq. (14), we get the standard deviation of the lifetime,

$$\begin{aligned} \sigma_\tau &= \frac{1 + \tau^2}{2 \sin(\pi a)} \left(\frac{1}{N_{\text{det}}} \frac{\pi a}{1 + 4\tau^2} \right)^{\frac{1}{2}} \\ &\quad \times (2\pi a - \sin(2\pi a) + 10\pi a\tau^2 - 3 \sin(2\pi a)\tau^2 + 8\pi a\tau^4)^{\frac{1}{2}}. \end{aligned} \quad (51)$$

Consequently, the F -value is calculated as

$$\begin{aligned} F &= \frac{1 + \tau^2}{2\tau \sin(\pi a)} \left(\frac{\pi a}{1 + 4\tau^2} \right)^{\frac{1}{2}} \\ &\quad \times (2\pi a - \sin(2\pi a) + 10\pi a\tau^2 - 3 \sin(2\pi a)\tau^2 + 8\pi a\tau^4)^{\frac{1}{2}}. \end{aligned} \quad (52)$$

By letting $a \rightarrow 0$, the F -value of a Dirac comb modulation can be directly obtained as

$$F = (1 + \tau^2) \left(\frac{1 + 2\tau^2}{1 + 4\tau^2} \right)^{\frac{1}{2}}. \quad (53)$$

For both cases, the normalized SNR can be calculated using Eq. (34). Figure 3 plots the F -values from these theoretical derivations and from the Monte Carlo simulations. The best figures of merit are $F = 1.00$, $\text{SNR} = 0.40$ for both the Dirac comb and the periodic square wave with a duty cycle $a = 0.001$. These two modulation waveforms have very similar F -value curves, as the duty cycle of the square wave is so small that it can be approximately regarded as a Dirac function. The optimal SNR performance can be achieved as long as

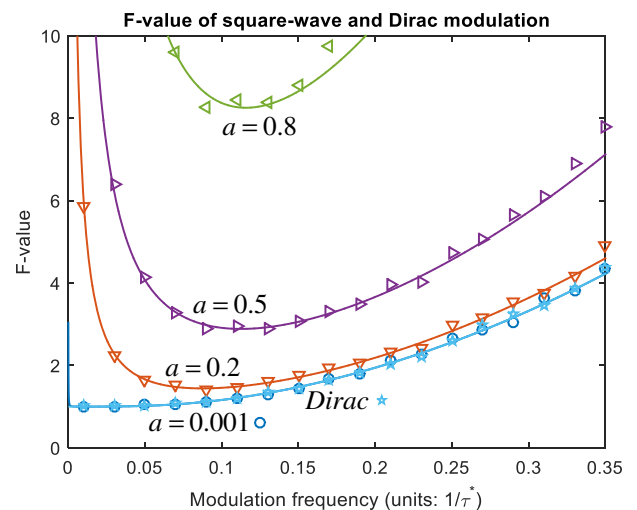


Fig. 3. F -value as a function of the modulation frequency with the first harmonic frequency (ω) lock-in detection for periodic square wave- and Dirac comb-modulated excitation light.

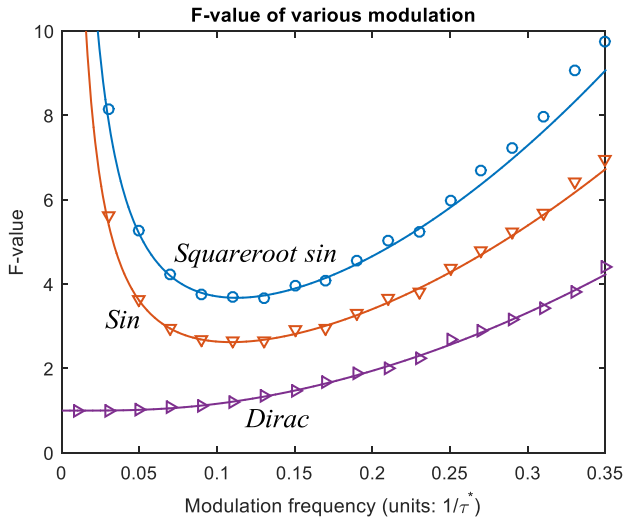


Fig. 4. F -value as a function of the modulation frequency with the first harmonic frequency (1ω) lock-in detection for excitation lights with various modulations.

the frequency is smaller than $0.04/\tau^*$, which is a band instead of a single frequency point. It can be seen from Fig. 3 that square waves with smaller duty cycles produce better F -values in this case.

D. Comparison

Figure 4 compares the F -values of the aforementioned modulation waveforms. The Dirac comb (or a periodic square wave with a very small duty cycle) has the best performance in SNR, while the square root of sinusoidal modulation is the worst. This phenomenon can be explained by Table 1, where the first harmonic Fourier coefficients a_1 for the effective exciting lights $\varepsilon(t)$ are listed and compared. The larger $|a_1|$ is, the better figures of merit this modulation has. This correlation between $|a_1|$ and the figures of merit is expected, because the detector only locks in the first harmonic frequency components G_1 and S_1 , which are directly related to a_1 by Eq. (6), to calculate the lifetime. While the noise, or uncertainty, in each modulation form is the same, the signal strength is stronger for the one with larger $|a_1|$; therefore, the SNR performance is positively correlated to the magnitude of a_1 . This analysis can be generalized to the lock-in of the n th harmonic component. Also from the comparison, the F -value for sinusoidal modulation with $m = 1$ is 2.62, which is led by the 2PE process of the fluorophores. This means that the number of photons needed to acquire a certain SNR is about 6.9 ($\approx 2.62^2$) times more than that of an ideal case. On the other hand, $F = 3.67$ of the corresponding one-photon excitation [23], which is equivalent to the two-photon square root of sinusoidal modulation here, requires

Table 1. Comparison of Modulation Waveforms

Waveform	min F	max $\overline{\text{SNR}}$	a_1	$ a_1 $
Square root Sin	3.67	0.11	$-\frac{1}{4\pi}i$	0.0796
Sin	2.62	0.15	$-\frac{1}{3\pi}i$	0.1061
Dirac	1.00	0.40	$\frac{1}{2\pi}$	0.1592

about 13.5 ($\approx 3.67^2$) times more photons to be collected than an ideal case. The 50% decrease in the required photon number shows a potential advantage in the SNR of two-photon microscopy over the conventional one-photon microscopy.

5. DETECTION SIGNAL-TO-NOISE RATIO ANALYSIS

The SNR performance of FD-FLIM is also limited by the detector lock-in implementation. In this section, we limit our discussion to sinusoidally modulated excitation light, for it is easy to produce and is commonly used to evaluate FD-FLIM [24].

The sinusoidal modulation has been described in Eqs. (35) and (36). The lock-in techniques can only exploit the DC and the first and second harmonic Fourier coefficients of $\varepsilon(t)$,

$$a_0 = \frac{1}{2\pi}, \quad a_1 = -\frac{m}{\pi(m^2 + 2)}i, \quad a_2 = -\frac{m^2}{4\pi(m^2 + 2)}. \quad (54)$$

With Eq. (6), we have

$$G_0 = \frac{1}{2\pi}, \quad S_0 = 0, \\ G_1 = -\frac{m}{\pi(m^2 + 2)}\frac{\tau}{1 + \tau^2}, \quad S_1 = -\frac{m}{\pi(m^2 + 2)}\frac{1}{1 + \tau^2}, \\ G_2 = -\frac{m^2}{4\pi(m^2 + 2)}\frac{1}{1 + 4\tau^2}, \quad S_2 = \frac{m^2}{4\pi(m^2 + 2)}\frac{2\tau}{1 + 4\tau^2}. \quad (55)$$

The lifetime τ can then be obtained by solving the equations above. Since these Fourier coefficients provide redundant knowledge of τ , a variety of combinations among them can be exploited to get τ .

A. 1ω Lock-In

The lifetime can be extracted by solely measuring G_1 and S_1 , which means that we only lock in the first harmonic frequency 1ω . Identical to the case discussed in Section 4.B, the lifetime is obtained with $\tau = G_1/S_1$, and the figures of merit are calculated from Eqs. (43) and (34).

B. 2ω Lock-In

The second harmonic (2ω) components G_2 and S_2 can also be used to determine the lifetime:

$$\tau = -\frac{1}{2}\frac{S_2}{G_2}, \quad (56)$$

which has the same form as Eq. (10). Therefore, Eqs. (10)–(14) still apply. Similar to Eqs. (20) and (21), denoting the random processes corresponding to G_2 and S_2 in the detector as X_{G2} and X_{S2} , respectively, the expected value of the acquired lifetime is

$$\bar{\tau} = -\frac{1}{2}\frac{N_{\text{det}}E[X_{S2}]}{N_{\text{det}}E[X_{G2}]}. \quad (57)$$

With the definition of Fourier transforms and from Eq. (5), we have

$$X_{G2} = \cos(2t), \quad X_{S2} = -\sin(2t), \quad (58)$$

and the expected values are

$$E[X_{G_2}] = \int_0^{2\pi} p(t) \cos(2t) dt = 2\pi G_2, \quad (59)$$

$$E[X_{S_2}] = -\int_0^{2\pi} p(t) \sin(2t) dt = 2\pi S_2. \quad (60)$$

With $U = -S_2/2$, $V = G_2$, we have

$$\begin{aligned} \mu_1 &= E[U] = -\frac{1}{2} N_{\det} E[X_{S_2}] = N_{\det} \frac{m^2}{2(m^2 + 2)} \frac{\tau}{1 + 4\tau^2}, \\ \mu_2 &= E[V] = N_{\det} E[X_{G_2}] = -N_{\det} \frac{m^2}{2(m^2 + 2)} \frac{1}{1 + 4\tau^2}. \end{aligned} \quad (61)$$

The variances and the correlation coefficient are

$$\begin{aligned} \sigma_1^2 &= E[U^2] = \frac{1}{4} N_{\det} E[X_{S_2}^2], \\ \sigma_2^2 &= E[V^2] = N_{\det} E[X_{G_2}^2], \\ \rho\sigma_1\sigma_2 &= E[UV] = -\frac{1}{2} N_{\det} E[X_{G_2}X_{S_2}]. \end{aligned} \quad (62)$$

From Eq. (5),

$$E[X_{S_2}^2] = E[\sin^2(2t)] = \frac{1}{2} (1 - 2\pi G_4), \quad (63)$$

$$E[X_{G_2}^2] = E[\cos^2(2t)] = \frac{1}{2} (1 + 2\pi G_4), \quad (64)$$

$$E[X_{G_2}X_{S_2}] = E[-\cos(2t) \sin(2t)] = \frac{1}{2} 2\pi S_4. \quad (65)$$

With Eq. (54), we know that $a_4 = 0$, and therefore $G_4 = 0$ and $S_4 = 0$. So,

$$\sigma_1^2 = \frac{1}{8} N_{\det}, \quad \sigma_2^2 = \frac{1}{2} N_{\det}, \quad \rho\sigma_1\sigma_2 = 0. \quad (66)$$

Then from Eq. (14), the standard deviation of τ can be calculated,

$$\sigma_\tau = \sqrt{\frac{1}{2N_{\det}} \frac{m^2 + 2}{m^2} (1 + 4\tau^2)^{\frac{3}{2}}}. \quad (67)$$

Consequently, the F -value is

$$F = \frac{m^2 + 2}{\sqrt{2}m^2} \frac{(1 + 4\tau^2)^{\frac{3}{2}}}{\tau}, \quad (68)$$

and the normalized SNR can be obtained with Eq. (34).

C. DC and 1 ω Lock-In

The lifetime can also be computed by the combination of DC (G_0) and 1 ω (S_1) components,

$$\tau = \left(-\frac{2m}{m^2 + 2} \frac{G_0}{S_1} - 1 \right)^{\frac{1}{2}}. \quad (69)$$

In this case, τ is not in the form of Eq. (10), so the aforementioned analysis in Eqs. (10)–(14) cannot be applied. However, the uncertainty in τ can still be obtained indirectly, with the approximate analysis method for a function of a random variable [39].

Generally, for two random variables X and Y with a functional relationship $Y = g(X)$, if we make two assumptions that (1) the function $g(X)$ is “relatively smooth” in the region

around the mean value μ_X of X , and (2) X has a small standard deviation σ_X ($\sigma_X < 1$), then $Y = g(X)$ can be Taylor expanded around the mean value μ_X and yields

$$\begin{aligned} Y &= g(X)|_{X=\mu_X} + (X - \mu_X) \left. \frac{dg}{dx} \right|_{X=\mu_X} \\ &+ \frac{1}{2!} (X - \mu_X)^2 \left. \frac{d^2g}{dx^2} \right|_{X=\mu_X} + \dots \end{aligned} \quad (70)$$

Taking the expected value of both sides of this equation, we get

$$E[Y] = g(\mu_X) + \frac{\sigma_X^2}{2} g''(\mu_X), \quad (71)$$

where the relation $E[X - \mu_X] = E[X] - \mu_X = 0$ has been used.

Specifically, in this case,

$$X = \frac{G_0}{S_1}, \quad Y = \tau = g(X) = \left(-\frac{2m}{m^2 + 2} X - 1 \right)^{\frac{1}{2}}. \quad (72)$$

We calculate the mean and standard deviation of X first. Since X is in the form of Eq. (10), Eqs. (10)–(14) can be applied to calculate μ_X and σ_X and $U = G_0$ and $V = S_1$. Denoting X_{G_0} as the random process corresponding to G_0 in the detector, and from Eq. (5), $X_{G_0} = \cos(0t) = 1$, whose expected value is

$$E[X_{G_0}] = \int_0^{2\pi} p(t) dt = 1. \quad (73)$$

With Eqs. (73) and (24), we have

$$\begin{aligned} \mu_1 &= E[U] = N_{\det} E[X_{G_0}] = N_{\det}, \\ \mu_2 &= E[V] = N_{\det} E[X_{S_1}] = -N_{\det} \frac{2m}{m^2 + 2} \frac{1}{1 + \tau^2}. \end{aligned} \quad (74)$$

Then, with Eq. (28), the variances and correlation coefficients are

$$\begin{aligned} \sigma_1^2 &= E[U^2] = N_{\det} E[X_{G_0}^2] = N_{\det}, \\ \sigma_2^2 &= E[V^2] = N_{\det} E[X_{S_1}^2] = N_{\det} \left[\frac{1}{2} + \frac{m^2}{4(m^2 + 2)} \frac{1}{1 + 4\tau^2} \right], \\ \rho\sigma_1\sigma_2 &= E[UV] = N_{\det} E[X_{S_1}] = -N_{\det} \frac{2m}{m^2 + 2} \frac{1}{1 + \tau^2}. \end{aligned} \quad (75)$$

Therefore, the moments of X can be calculated from Eqs. (12)–(14),

$$\begin{aligned} \mu_X &= -\frac{m^2 + 2}{2m} (1 + \tau^2) \left\{ 1 - \frac{1}{N_{\det}} + \frac{1}{N_{\det}} \left(\frac{m^2 + 2}{2m} \right)^2 \right. \\ &\times \left. (1 + \tau^2)^2 \left[\frac{1}{2} + \frac{m^2}{4(m^2 + 2)} \frac{1}{1 + 4\tau^2} \right] \right\}, \end{aligned} \quad (76)$$

$$\begin{aligned} \sigma_X^2 &= \frac{1}{N_{\det}} \left(\frac{m^2 + 2}{2m} \right)^2 (1 + \tau^2)^2 \left\{ -1 + \left(\frac{m^2 + 2}{2m} \right)^2 \right. \\ &\times \left. (1 + \tau^2)^2 \left[\frac{1}{2} + \frac{m^2}{4(m^2 + 2)} \frac{1}{1 + 4\tau^2} \right] \right\}. \end{aligned} \quad (77)$$

From Eq. (72), the second derivative of $g(X)$ yields

$$g''(X) = -\frac{m^2}{(m^2 + 2)^2} \left(-\frac{2m}{m^2 + 2} X - 1 \right)^{-\frac{3}{2}}. \quad (78)$$

Consequently, based on Eq. (71), the mean value of Y (or τ) is

$$E[\tau] = \left(\frac{-2m}{m^2 + 2} \mu_X - 1 \right)^{\frac{1}{2}} - \frac{m^2 \sigma_X^2}{2(m^2 + 2)^2} \left(\frac{-2m}{m^2 + 2} \mu_X - 1 \right)^{-\frac{3}{2}}. \quad (79)$$

We know that the mean square value of τ is

$$E[\tau^2] = E \left[-\frac{2m}{m^2 + 2} X - 1 \right] = -\frac{2m}{m^2 + 2} \mu_X - 1, \quad (80)$$

so the standard deviation of the acquired lifetime can be calculated from

$$\sigma_\tau = (E[\tau^2] - E[\tau]^2)^{\frac{1}{2}}, \quad (81)$$

and accordingly, the figures of merit can be obtained using Eqs. (7) and (34).

D. Comparison

Figure 5 plots the F -values from the theoretical results in Sections 5.A–5.C along with the Monte Carlo simulations. The best figures of merit for 1ω lock-in detection have been discussed in Section 4.B; these are $F = 2.62$, $\text{SNR} = 0.15$ at the frequency of $0.11/\tau^*$. This indicates that the optimal 1ω detection requires 6.9 ($\approx 2.62^2$) times more photons to achieve the same SNR as the ideal case. For 2ω lock-in, the SNR performance is much worse, resulting in $F = 11.02$, $\text{SNR} = 0.04$ at the frequency of $0.06/\tau^*$. However, the combination of DC and 1ω lock-in detection shows an improved figure of merit of $F = 1.87$, $\text{SNR} = 0.21$ at the frequency of $0.14/\tau^*$. This means that the DC and 1ω combination only needs to collect 3.5 ($\approx 1.87^2$) times more photons to achieve the same SNR level as the ideal case, which corresponds to a $2 \times$ improvement in the acquisition rate relative to the traditional 1ω -only lock-in detection method. The combined DC and 1ω lock-in approach is superior to the single-frequency lock-in method for modulation frequencies greater than $0.06/\tau^*$. This allows for a wide range of high-performance modulation

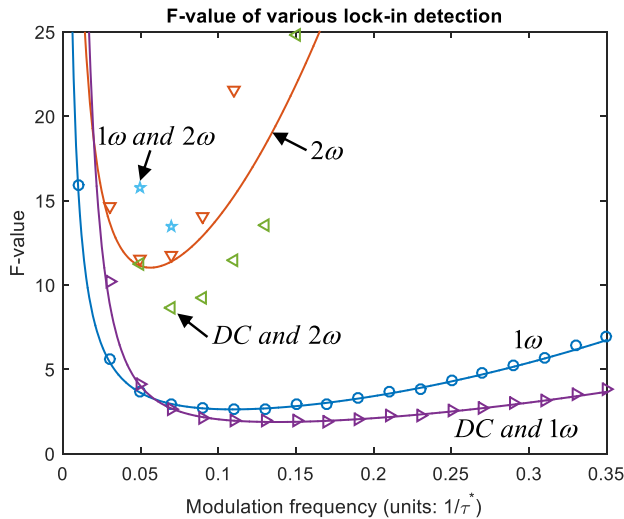


Fig. 5. F -value as a function of the modulation frequency with various lock-in detection techniques for sinusoidally modulated excitation light.

frequencies, which is important for experimental design and implementation.

Solving Eq. (55) indicates that lifetime measurements are possible using DC + 2ω and $1\omega + 2\omega$ combinations,

$$\tau = \frac{1}{2} \left[-\frac{m^2}{2(m^2 + 2)} \frac{G_0}{G_2} - 1 \right]^{\frac{1}{2}}, \quad \text{for DC and } 2\omega, \quad (82)$$

$$\tau = \left(\frac{m - 4 \frac{G_2}{S_1}}{16 \frac{G_2}{S_1} - m} \right)^{\frac{1}{2}}, \quad \text{for } 1\omega \text{ and } 2\omega. \quad (83)$$

However, the uncertainty in these methods cannot be extracted from Eqs. (82) and (83) using the analytical methods presented in this paper, and the Monte Carlo simulations indicate a poor SNR (Fig. 5).

Since the noise in this system is predominantly determined by photon quantum noise, the noise spectrum can be assumed to be white, i.e., independent of the modulation frequency, up to a limit set by the bandwidths of the detectors and amplifiers [34,36,40]. To achieve a high SNR, the frequency components with the largest magnitude should be employed (regardless of frequency). Although the DC component has the largest magnitude, it does not contain lifetime information. Therefore, the combination of DC and 1ω lock-in will result in the best SNR. The lock-in techniques exploiting the weak 2ω signal, on the other hand, will have poor SNR performance.

6. DISCUSSION OF EXPERIMENTAL PERFORMANCE

To date, lifetime microscopy performance analysis assumes that only one 2PE fluorescent photon is emitted in every modulation period, as indicated by the normalization in Eq. (19); i.e., the 2PE emission rate is assumed to be an arbitrary constant. However, the emission rate is limited by the spontaneous emission rate (i.e., fluorescence saturation), which is independent of the modulation period. 2PE microscopes typically operate at as high of an excitation rate as possible while avoiding saturation to achieve maximum SNR, for saturation could complicate the excited-state dynamics and alter the measured lifetime. Therefore, a useful comparison for 2PE FLIM performance would be in the limit of constant fluorescence emission.

To compare the performance at a constant emission rate, we renormalize the excitation light to avoid the fluorescence saturation. Instead of using Eq. (19), we define a maximally allowed fluorescence intensity P_{\max} such that

$$p(t) \leq P_{\max}. \quad (84)$$

With this new normalization criterion, the excitation light signal previously described by Eqs. (15), (35), and (44) now changes to

$$e(t) = \left(\frac{P_{\max}}{1 + m} \right)^{\frac{1}{2}} [1 + m \sin(t)]^{\frac{1}{2}}, \quad (85)$$

$$e(t) = \left[\frac{P_{\max}}{2(1 + m)^2} \right]^{\frac{1}{2}} [1 + m \sin(t)], \quad (86)$$

$$e(t) = \sum_{k=-\infty}^{\infty} \left[P_{\max} \frac{1 - \exp\left(-\frac{2\pi}{\tau}\right)}{1 - \exp\left(-\frac{2\pi a}{\tau}\right)} \right]^{\frac{1}{2}} \times [\theta(t - 2\pi k + \pi a) - \theta(t - 2\pi k - \pi a)], \quad (87)$$

respectively. Note that the Dirac comb modulation is not possible in this normalization, as the saturation limit condition has negated the infinite intensity of Dirac pulses.

This new normalization criterion does not affect the F -value described in Eq. (7), which is independent of the fluorescence intensity; however, the normalized SNR, which was defined in Eq. (9), will be altered. In Fig. 6, we present theoretically calculated SNRs of various modulation schemes for the 1ω lock-in detection (curves) with Monte Carlo simulations (dots), under two different normalization criteria, Eqs. (19) and (84). The saturation-limited normalization in Eq. (84) prevents the emission rate from exceeding the maximally allowed value of the fluorophores. As can be seen from Fig. 6, the square wave's

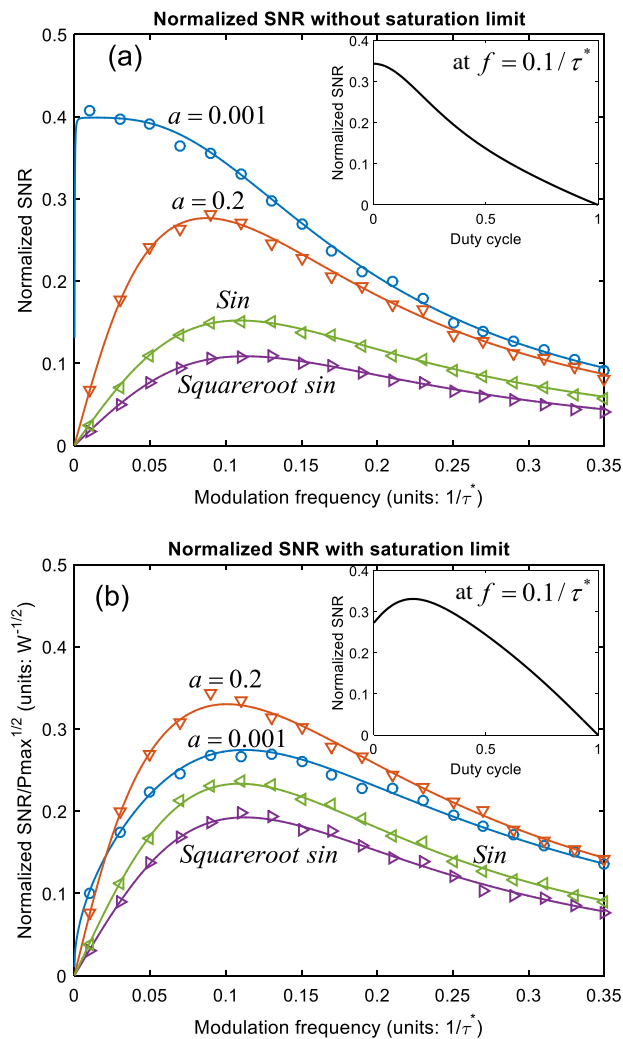


Fig. 6. Normalized SNR as a function of the modulation frequency with the first harmonic frequency (1ω) lock-in detection when (a) the saturation limit is not considered and (b) the saturation limit is taken into account. Insets: the square wave modulation's best normalized SNR as a function of the duty cycle a at the modulation frequency of $0.1/\tau^*$.

duty cycle a now affects $\overline{\text{SNR}}$ differently. For example, when not limited by saturation, as in Fig. 6(a), the $\overline{\text{SNR}}$ decreases with the increasing duty cycle, while in the case of saturation [Fig. 6(b)], the optimal SNR is found at $a = 0.175$, rather than the smallest a (e.g. $a = 0.001$), as suggested in Section 4.C.

7. CONCLUSION

We have presented analytical and simulated SNR figures of merit for MPM-FD-FLIM methods. The comparison in figures of merit between the square root of the sinusoidal and the sinusoidal modulations theoretically confirms that the MPM-FD-FLIM has a superior SNR performance compared to conventional one-photon FD-FLIM, which has not been previously described theoretically. Our analysis shows that 50% fewer photons are required in MPM-FD-FLIM to achieve the same SNR as one-photon FD-FLIM.

We have also shown that employing more harmonic components allows for an improved SNR compared to conventional single-frequency lock-in detection, as is typically used in FD-FLIM. For example, the generally discarded DC signal can not only be used in FLIM, but also greatly improves SNR performance. The combination of DC and 1ω components increases the lifetime measurement rate by a factor of 2 compared to traditional fundamental frequency FD-FLIM.

Finally, this work can act as a guideline for experimentalists using MPM-FD-FLIM. To get the best SNR performance, periodic square-wave modulation with a small duty cycle (e.g., $a < 0.2$) with a frequency of $f \approx 0.1/\tau^*$ is preferred. As fluorophore saturation is common in MPM, a 0.175 duty cycle modulated at $f \approx 0.1/\tau^*$ is recommended for the maximal SNR. Nevertheless, square-wave modulation may be a problem for systems with limited bandwidth, especially for those requiring a high modulation frequency. If bandwidth limitation is indeed a problem, the sinusoidal modulation at $f \approx 0.1/\tau^*$ detailed in this paper is always recommended due to its easy implementation and the potential to get an F -value as low as 1.87 using the combined DC and 1ω lock-in technique presented in this paper.

In conclusion, we have presented for the first time a theoretical framework for MPM-FD-FLIM SNR optimization at both the source and the detector and the data analysis techniques for improved SNR over the current conventional methods.

Funding. National Science Foundation (NSF) (CBET-1554516).

REFERENCES

1. W. R. Zipfel, R. M. Williams, and W. W. Webb, "Nonlinear magic: multiphoton microscopy in the biosciences," *Nat. Biotechnol.* **21**, 1369–1377 (2003).
2. J. Mertz, "Nonlinear microscopy: new techniques and applications," *Curr. Opin. Neurobiol.* **14**, 610–616 (2004).
3. F. Helmchen and W. Denk, "Deep tissue two-photon microscopy," *Nat. Methods* **2**, 932–940 (2005).
4. K. Svoboda and R. Yasuda, "Principles of two-photon excitation microscopy and its applications to neuroscience," *Neuron* **50**, 823–839 (2006).

5. A. Cheng, J. T. Gonçalves, P. Golshani, K. Arisaka, and C. Portera-Cailliau, "Simultaneous two-photon calcium imaging at different depths with spatiotemporal multiplexing," *Nat. Methods* **8**, 139–142 (2011).
6. G. Palczewska, Z. Dong, M. Golczak, J. J. Hunter, D. R. Williams, N. S. Alexander, and K. Palczewski, "Noninvasive two-photon microscopy imaging of mouse retina and retinal pigment epithelium through the pupil of the eye," *Nat. Med.* **20**, 785–789 (2014).
7. G. D. Vigil, A. J. Adami, T. Ahmed, A. Khan, S. Chapman, B. Andemariam, R. S. Thrall, and S. S. Howard, "Label-free and depth resolved optical sectioning of iron-complex deposits in sickle cell disease splenic tissue by multiphoton microscopy," *J. Biomed. Opt.* **20**, 066001 (2015).
8. W. Denk, J. H. Strickler, and W. W. Webb, "Two-photon laser scanning fluorescence microscopy," *Science* **248**, 73–76 (1990).
9. J. Mertz, C. Xu, and W. W. Webb, "Single-molecule detection by two-photon-excited fluorescence," *Opt. Lett.* **20**, 2532 (1995).
10. M. Sonnleitner, G. Schütz, and T. Schmidt, "Imaging individual molecules by two-photon excitation," *Chem. Phys. Lett.* **300**, 221–226 (1999).
11. G. H. Patterson and D. W. Piston, "Photobleaching in two-photon excitation microscopy," *Biophys. J.* **78**, 2159–2162 (2000).
12. F. Cannone, G. Chirico, and A. Diaspro, "Two-photon interactions at single fluorescent molecule level," *J. Biomed. Opt.* **8**, 391–395 (2003).
13. A. Diaspro, G. Chirico, and M. Collini, "Two-photon fluorescence excitation and related techniques in biological microscopy," *Q. Rev. Biophys.* **38**, 97–166 (2005).
14. E. E. Hoover and J. A. Squier, "Advances in multiphoton microscopy technology," *Nat. Photonics* **7**, 93–101 (2013).
15. G. Weber, "Resolution of the fluorescence lifetimes in a heterogeneous system by phase and modulation measurements," *J. Phys. Chem.* **85**, 949–953 (1981).
16. K. Carlsson and A. Liljeborg, "Confocal fluorescence microscopy using spectral and lifetime information to simultaneously record four fluorophores with high channel separation," *J. Microsc.* **185**, 37–46 (1997).
17. C. J. De Grauw and H. C. Gerritsen, "Multiple time-gate module for fluorescence lifetime imaging," *Appl. Spectrosc.* **55**, 670–678 (2001).
18. H. C. Gerritsen, A. Draaijer, D. J. van den Heuvel, and A. V. Agronskaia, "Fluorescence lifetime imaging in scanning microscopy," in *Handbook of Biological Confocal Microscopy*, J. Pawley, ed., 3rd ed. (Springer, 2006), pp. 516–534.
19. C.-W. Chang, D. Sud, and M.-A. Mycek, "Fluorescence lifetime imaging microscopy," *Methods Cell Biol.* **81**, 495–524 (2007).
20. J. D. Driscoll, A. Y. Shih, S. Iyengar, J. J. Field, G. A. White, J. A. Squier, G. Cauwenberghs, and D. Kleinfeld, "Photon counting, censor corrections, and lifetime imaging for improved detection in two-photon microscopy," *J. Neurophysiol.* **105**, 3106–3113 (2011).
21. Y. J. Won, S. Moon, W.-T. Han, and D. Y. Kim, "Referencing techniques for the analog mean-delay method in fluorescence lifetime imaging," *J. Opt. Soc. Am. A* **27**, 2402–2410 (2010).
22. Y. J. Won, W.-T. Han, and D. Y. Kim, "Precision and accuracy of the analog mean-delay method for high-speed fluorescence lifetime measurement," *J. Opt. Soc. Am. A* **28**, 2026–2032 (2011).
23. J. Philip and K. Carlsson, "Theoretical investigation of the signal-to-noise ratio in fluorescence lifetime imaging," *J. Opt. Soc. Am. A* **20**, 368–379 (2003).
24. Y. Lin and A. F. Gmitro, "Statistical analysis and optimization of frequency-domain fluorescence lifetime imaging microscopy using homodyne lock-in detection," *J. Opt. Soc. Am. A* **27**, 1145–1155 (2010).
25. A. A. Khan, S. K. Fullerton-Shirey, and S. S. Howard, "Easily prepared ruthenium-complex nanomicelle probes for two-photon quantitative imaging of oxygen in aqueous media," *RSC Adv.* **5**, 291–300 (2015).
26. D. O'Connor, *Time-Correlated Single Photon Counting* (Academic, 2012).
27. R. M. Ballew and J. N. Demas, "An error analysis of the rapid lifetime determination method for the evaluation of single exponential decays," *Anal. Chem.* **61**, 30–33 (1989).
28. G. I. Redford and R. M. Clegg, "Polar plot representation for frequency-domain analysis of fluorescence lifetimes," *J. Fluoresc.* **15**, 805–815 (2005).
29. J. Lecoq, A. Parpaleix, E. Roussakis, M. Ducros, Y. G. Houssen, S. A. Vinogradov, and S. Charpak, "Simultaneous two-photon imaging of oxygen and blood flow in deep cerebral vessels," *Nat. Med.* **17**, 893–898 (2011).
30. M. A. Yaseen, S. Sakadžić, W. Wu, W. Becker, K. A. Kasischke, and D. A. Boas, "In vivo imaging of cerebral energy metabolism with two-photon fluorescence lifetime microscopy of NADH," *Biomed. Opt. Express* **4**, 307–321 (2013).
31. S. S. Howard, A. Straub, N. Horton, D. Kobat, and C. Xu, "Frequency multiplexed in vivo multiphoton phosphorescence lifetime microscopy," *Nat. Photonics* **7**, 33–37 (2013).
32. S. Sakadžić, E. Roussakis, M. A. Yaseen, E. T. Mandeville, V. J. Srinivasan, K. Arai, S. Ruvinskaya, A. Devor, E. H. Lo, S. A. Vinogradov, and D. A. Boas, "Two-photon high-resolution measurement of partial pressure of oxygen in cerebral vasculature and tissue," *Nat. Methods* **7**, 755–759 (2010).
33. A. Elder, S. Schlachter, and C. F. Kaminski, "Theoretical investigation of the photon efficiency in frequency-domain fluorescence lifetime imaging microscopy," *J. Opt. Soc. Am. A* **25**, 452–462 (2008).
34. K. Carlsson, "Signal-to-noise ratio for confocal microscopy when using the Intensity-modulated Multiple-beam Scanning (IMS) technique," *Micron* **26**, 317–322 (1995).
35. K. Carlsson, "Theoretical investigation of the signal-to-noise ratio for different fluorescence lifetime imaging techniques," *Proc. SPIE* **4622**, 70–78 (2002).
36. K. Carlsson and A. Liljeborg, "Simultaneous confocal lifetime imaging of multiple fluorophores using the intensity-modulated multiple-wavelength scanning (IMS) technique," *J. Microsc.* **191**, 119–127 (1998).
37. A. Esposito, H. C. Gerritsen, and F. S. Wouters, "Optimizing frequency-domain fluorescence lifetime sensing for high-throughput applications: photon economy and acquisition speed," *J. Opt. Soc. Am. A* **24**, 3261–3273 (2007).
38. D.-U. Li, E. Bonnist, D. Renshaw, and R. Henderson, "On-chip, time-correlated, fluorescence lifetime extraction algorithms and error analysis," *J. Opt. Soc. Am. A* **25**, 1190–1198 (2008).
39. H. Benaroya, S. M. Han, and M. Nagurka, *Probabilistic Models for Dynamical Systems*, 2nd ed. (CRC Press, 2013).
40. E. Gratton, D. M. Jameson, and R. D. Hall, "Multifrequency phase and modulation fluorometry," *Annu. Rev. Biophys. Bio.* **13**, 105–124 (1984).